Magnetic Behavior of γ-Fe_2O_3 Nanocrystals Dispersed in Colloidal Silica Particles

Pedro Tartaj,* Teresita González-Carreño, and Carlos J. Serna

Instituto de Ciencia de Materiales de Madrid, CSIC, Cantoblanco, 28049, Madrid, Spain

Received: May 8, 2002; In Final Form: October 11, 2002

The magnetic properties of composites that consisted of γ-Fe_2O_3 nanocrystals (4−10 nm) dispersed in submicrometer spherical silica particles at different packing fractions have been studied. The spherical composites were prepared by aerosol pyrolysis of a methanol solution containing tetraethoxysilane and iron nitrate and further annealing in a conventional furnace. Hysteresis loops registered at room temperature indicated that all composites exhibited superparamagnetic behavior. Studies of the thermal evolution of magnetization indicated that these composites could be considered as an adequate experimental system to determine the influence of particle size and interparticle interactions on the magnetic properties. It was observed that the blocking temperature strongly depends on particle size. Also, we have found that interparticle interactions cause frustration of the moments, and we have determined a dependence of the effective anisotropy with the particle size probably associated with the existence of surface anisotropy.

Introduction

Nanocrystalline magnetic materials often reveal unique properties that differ from their bulk polycrystalline counterparts. Interest in this area comes partly from data storage technology (e.g., hard disk drives[1]) and partly because nanomagnets provide a highly controlled experimental system for fundamental studies.[2−6] Many of the unique magnetic properties of nanostructured materials are due to finite size effect and/or the high surface/volume ratio, thus making the study of the interrelation between microstructure and magnetism very appealing.[7,8] Particularly interesting physics occurs when nanomagnets are dispersed in nonmagnetic matrixes. The magnetic behavior of these systems can vary widely depending on the size of the nanocrystalline particles as well as on the packing fraction and the interaction between the nanomagnets and the matrixes.[9−12]

In general, fine particle systems are composed of a collection of different-sized single domain particles. All particle moments are blocked at the lowest temperatures; however, with increasing temperature, the smaller particle moments will become superparamagnetic, moments of intermediate-sized particles will undergo collective excitations, and the moments in the largest particles will remain blocked. The wide variety of magnetic behavior of nanostructured materials is further complicated by interparticle interactions arising from the difficulty in controlling particle dispersion. For sufficiently dilute dispersions, interparticle interactions (usually of a dipolar nature) are negligible and the crossover to the blocked state with decreasing temperature depends only on the physical properties of the individual particles. However, at higher densities, interparticle interactions strongly affect the behavior of the dispersion. In particular, dipolar interactions between particles cause frustration of the moments, which no longer align themselves precisely with the particles' easy axes at low *T*. Rather, as the dispersion is cooled, collective, glassy behavior results. While this phenomenon has been studied extensively, most work to date has centered on shifts of the blocking temperature and the subtle question of whether the cooperative freezing can be described as a true thermodynamic spin glass transition.[13]

Knowledge of these fundamental properties is essential for creative use of magnetic composites containing nanocrystals that can have tremendous potential and lead to improved materials for applications in biology and medicine for the separation of biochemical products and cells,[14] magnetic resonance imaging contrast enhancement,[15] and tissue specific release of therapeutic agents.[16] All of these applications depend on a magnetic material with a modified surface that provides functionality to the composite. In this way, the dispersion of nanomagnets in silica matrixes that can be easily activated to provide functionality to the magnetic material seems the ideal encapsulating material.[17] In addition, the silica matrix allows a fine-tuning with temperature of the magnetic properties.[12,18] In particular, for the magnetically assisted chemical separation (MACS) of biochemical products and cells, the use of γ-Fe_2O_3 nanocrystals homogeneously dispersed in microspherical silica cages could be very effective (microspherical particles are expected to be stable against sedimentation in the absence of a magnetic field).[19]

In this paper, we report a detailed study of the magnetic properties of γ-Fe_2O_3 nanocrystals (4−10 nm) dispersed inside colloidal silica spherical particles (average size ∼150 nm in diameter). The composites were synthesized by an aerosol-assisted method. We have analyzed the thermal dependence of the macroscopic magnetic parameters to elucidate how factors such as the particle size and the content of magnetic material affect the magnetic response of the composites.

Experimental Section

Synthesis of Magnetic Composites. The composites were prepared by an aerosol-assisted method. Details of the preparation can be found elsewhere.[12,19] Briefly, tetraethoxysilane (TEOS) and iron nitrate in the right proportions were dissolved in methanol at a total salt concentration of 1 M. Then, the solutions were atomized at 1.6 mL min^{-1} with an air pressure of 1.7 kg cm^{-2} and directed to a first furnace kept at 250 °C to

* To whom correspondence should be addressed. E-mail: ptartaj@icmm.csic.es.

10.1021/jp0260898 CCC: $25.00
Published on Web 12/10/2002

TABLE 1: Volume Packing Fraction (PF), Heating Temperature, Particle Size Determined by TEM (D_{TEM}), Crystallite Size (D_{XR}), Magnetic Size (D_{Mag}) Determined Following the Method of Chantrell et al.,[20] and M_S at Room Temperature[a]

sample	PF (%)	heating temp (°C)	D_{TEM} (nm)	D_{XR} (nm)	M_S (emu/g Fe_2O_3)	D_{Mag} (nm)
F1	20	1000	9 (3)	9 (1)	49	8.8
F2	20	950	7 (2)	6.6 (0.8)	38	6.2
F3	20	800	4 (1)	4.2 (0.5)	25	3.9
F4	10	900	4 (1)	4.3 (0.5)	25	3.7
F5	5	1050	4 (1)	3.7 (0.4)	24	3.8

[a] PF was obtained from the wt % content in samples by considering the density of γ-Fe_2O_3 (~5.5 g/cm^3) and SiO_2 (~2.5 g/cm^3).

favor the evaporation of the solvent and therefore the precipitation of solute. The solid aerosol was then decomposed in a second furnace, which was held at 500 °C. The powders so generated were further heated in a conventional furnace for 2 h at different temperatures in air to produce γ-Fe_2O_3 nanocrystals of different particle size. Details of the iron oxide content and heating temperatures used for the preparation of the samples are given in Table 1.

Characterization Techniques. The different phases present in the solids were assessed by X-ray diffraction (XRD, PW1710, Philips). Crystallite sizes were calculated from the full width at half-maximum of the (311) reflection using the Scherrer equation. The morphology and size of the particles were examined by transmission electron microscopy (TEM, 2000 FX2, JEOL).

Magnetic properties of the samples were recorded in a vibrating sample magnetometer (model VTI, Oxford Instruments). The saturation magnetization (M_S) and coercivity field values (H_C) were obtained from the hysteresis loops registered up to a field of 7 T. M_S values were determined by H^{-1} extrapolation at high fields where a linear increase in the magnetization was observed. The temperature dependence of the magnetization was monitored by zero field-cooled (ZFC) and field-cooled (FC) experiments. The ZFC curve was obtained by first cooling the system in a zero magnetic field. The magnetic field was then applied (200 G), and the magnetization was measured while the temperature was increased. The FC curve was obtained in a similar way except that the sample was cooled in the measuring field (200 G).

Results and Discussion

Evidences of the formation of only γ-Fe_2O_3 were obtained by XRD (Figure 1). A typical microstructure of the composites showing γ-Fe_2O_3 nanospherical particles dispersed inside the spherical silica particles is displayed in Figure 2. A summary of the chemical composition and the main physical characteristics of the samples can be found in Table 1.

Hysteresis loops registered at room temperature show that all samples exhibit superparamagnetic behavior (i.e., zero coercivity field). M_S values (normalized to the γ-Fe_2O_3 content) were, in all cases, lower than that of bulk γ-Fe_2O_3 (75 emu/g), which reflects the small particle size of the γ-Fe_2O_3 nanocrystals (Table 1). Spin canting at the surface and/or the interior of the particles has been reported as being responsible for the reduction in M_S manifested by nanoparticles.[7] Supporting this interpretation, M_S values increased with the crystallite size, and for the samples with different packing fraction (i.e., different composition) but similar crystallite size, M_S values (normalized to the iron oxide content) were similar (Table 1). The fact that all of the characterized samples were superparamagnetic allowed us

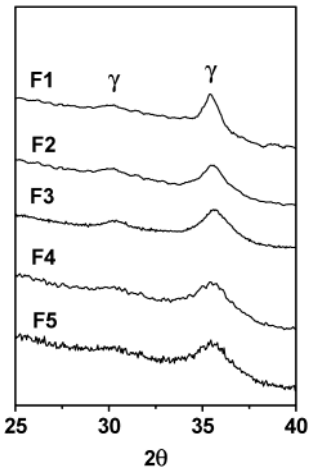

Figure 1. XRD patterns showing the presence of only γ-Fe_2O_3 in all samples.

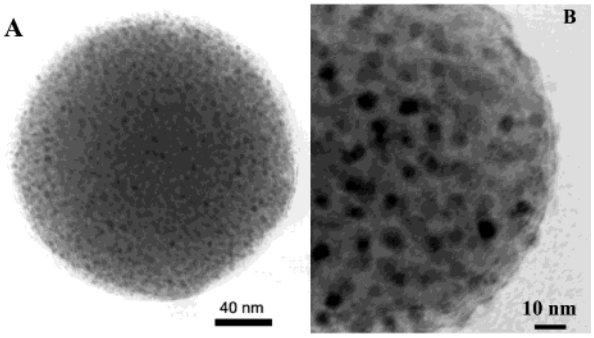

Figure 2. (A) TEM picture of a typical microstructure showing γ-Fe_2O_3 nanocrystals (dark spots) dispersed in spherical colloidal silica particles. (B) Details of a typical microstructure showing the nearly spherical shape of the γ-Fe_2O_3 nanocrystals (dark spots).

to estimate the magnetic size distribution parameters following the method of Chantrell et al.,[20] which uses magnetic measurements in low and high fields to obtain a fit to a sum of Langevin equations. As observed, the average particle size determined with this method is similar to that determined by XRD and TEM, which shows that each particle behaves as a single, coherent, thermally fluctuating moment (i.e., the physical and magnetic volumes of particles are similar).

The ZFC magnetization process exhibits the typical features of an assembly of magnetic particles with a distribution of blocking temperatures (Figure 3). This property is characterized by the existence of a broad maximum, indicating that the magnetic moment of each particle becomes blocked in the direction determined by its easy magnetization axis at a given temperature T_B. This temperature depends on particle volume, anisotropy, and orientation with respect to the applied field. An increase of the temperature at which the ZFC peak reaches its cusp, T_M, is evident as the γ-Fe_2O_3 crystallite size increases (Figure 3, Tables 1 and 2). Interparticle interactions (usually of a dipolar nature) will affect the effective anisotropy energy and change the temperature at which a particle becomes superparamagnetic. Normally, a shift of T_M to high temperature, due to an increase in relaxation times, is detected.[21,22] In our system, an increase in T_M is observed with the increase of packing fraction, which must be associated with the increase in the interparticle interactions (Figure 3, Tables 1 and 2). Because the particles in the sample have a certain distribution of volumes, each one of them becomes blocked at a different temperature, giving rise to a distribution of blocking temperatures (broadening

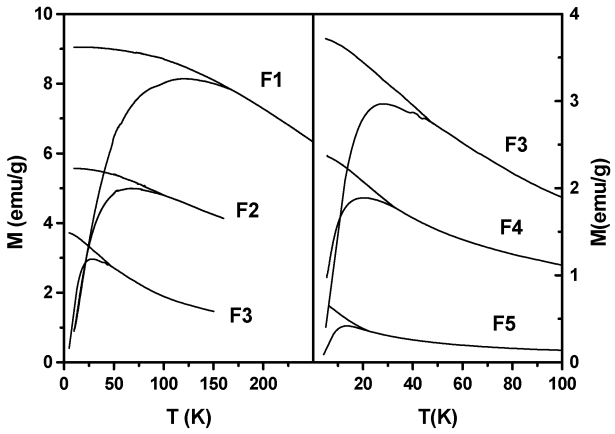

Figure 3. ZFC−FC magnetization as a function of temperature with an external applied field of 200 Oe for all samples.

TABLE 2: Values of T_M and T_S Obtained from the ZFC−FC Curves, Values of $M_R(0)/M_S(0)$, $\langle T_B \rangle$, and σ_y Obtained from the Fit of the Decay of the Reduced Remanence, Values of K_{eff} Obtained from the Law of Approach to Saturation, and Values of H_C Obtained from the Hysteresis Loops Registered at 5 K[a]

sample	T_M (K)	T_S (K)	$M_R(0)/M_S(0)$	$\langle T_B \rangle$ (K)	σ_y (nm)	K_{eff} ($\times 10^6$ erg/cm^3)	H_C (Oe)
F1	120	170	0.49	36	1.15	1.3	302
F2	67	95	0.43	23	1.10	2.0	351
F3	28	47	0.37	9	1.00	3.4	385
F4	20	33	0.42	8	1.00	3.3	371
F5	14	22	0.45	9	0.95	3.5	363

[a] The uncertainties are about 0.02 for $M_R(0)/M_S(0)$, 0.1 for the standard deviation, 1−2 K for $\langle T_B \rangle$, and 10−15% for the effective anisotropy constants.

of the ZFC magnetization curve). The fact that the curves become broader as the particle size increases reflects an increase in size dispersion. Above T_M, the magnetization decreases as the system enters into the superparamagnetic regime.

Under an applied magnetic field at room temperature, the magnetization direction of all magnetic moments aligns along the field direction, regardless of the easy axis direction of each individual nanoparticle. As the nanoparticles are cooled to very low temperatures in the presence of a magnetic field (FC), the magnetization direction of each particle is frozen in the field direction. Therefore, the magnetization displays a maximum at the lowest temperature in the FC process. The temperature at which the ZFC and FC curves start to separate (T_S) corresponds to the blocking of the largest particles. The difference between T_S and T_M is therefore a qualitative measure of the width of the energy barrier distribution and thus of the nanoparticles size distribution.[23,24] FC curves for the samples are also displayed in Figure 3. The difference $T_S - T_M$ (Figure 3, Tables 1 and 2) increased with the increase in particle size (i.e., heating temperature). This result manifests that the growing process of the iron oxide nanoparticles is not homogeneous. Likely, the iron oxide nanoparticles closer to the surface of the colloidal silica particles diffuse faster than those located closer to the center; therefore, the growing process is favored in this area, which causes the broadening of the size distribution. The increase in $T_S - T_M$ with the volume packing fraction (Figure 3, Tables 1 and 2) can be explained by the presence of a higher number of iron oxide nanocrystals that increase the probability of inhomogeneous growing processes.

Figure 4 shows the reduced remanence data as a function of temperature for all of the samples. We have analyzed the results

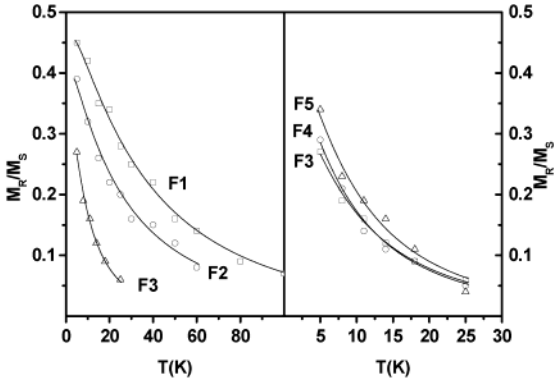

Figure 4. Variation of the reduced isothermal remanence with temperature for all of the samples. The solid lines represent the best fit of the data with a standard decay of remanence model.

using the standard relation for the temperature variation of the reduced remanence (normalized to the measured saturation magnetization) given by[21]

$$\frac{M_R(T)}{M_S(T)} = \frac{M_R(0)}{M_S(0)} \int_{T/\langle T_B \rangle}^{\infty} f(y)\, dy \qquad (1)$$

where $\langle T_B \rangle$ is the mean blocking temperature, $y = T_B/\langle T_B \rangle$ is the reduced blocking temperature, and $M_R(0)/M_S(0)$ is the reduced remanence at 0 K. The distribution $f(y)$ of reduced blocking temperatures is assumed to be a log-normal function.

$$f(y) = \frac{1}{(2\pi)^{1/2}\sigma_y} \exp\left[-\frac{(\ln y)^2}{2\sigma_y^2}\right] \qquad (2)$$

The best fits with eq 1 to the data are shown by the lines in Figure 4, and the values of the free parameters $M_R(0)/M_S(0)$, $\langle T_B \rangle$, and the standard deviation σ_y are given in Table 2. When the external field is turned off, the system displays a finite value of the remanence magnetization, M_R, which in the framework of the Stoner−Wohlfarth model is given by $M_R = 1/2(S_B M_S)$.[25] In the ideal case of well-separated fine particles, $S_B = 1$, and $M_R = M_S/2$ at $T = 0$ K, because the magnetic moments are randomly oriented over the hemisphere defined by the applied field and $\langle \cos\theta \rangle = 1/2$. However, in systems of interacting particles, the extrapolated remanence is expected to be lower because of more or less complete flux closure.[26] Thus, the fact that $M_R(0)/M_S(0)$ values are below 0.5 (Table 2) could be understood simply from the effect of competition between interparticle interactions and intraparticle anisotropy on the spin relaxation process, which produces frustration.[27] In agreement, for a given particle size (samples F3, F4, and F5), we observed a decrease in $M_R(0)/M_S(0)$ values with the increase in volume packing fraction (Table 2). For the samples with the same iron oxide content (F1, F2, and F3), an increase in the value of $M_R(0)/M_S(0)$ was detected with the increase in crystallite size (Tables 1 and 2), which can also be explained in terms of interactions among nanomagnets. Roughly, the separation distance, D, between particles can be expressed by the expression $D = d(1/X^{1/3} - 1)$, where d is the particle size and X is the volume packing fraction (i.e., bigger particle sizes involve larger distance between particles). Therefore, the observed increase in $M_R(0)/M_S(0)$ values with the particle size is also associated with a decrease in interparticle interactions.

As expected, the values of $\langle T_B \rangle$ decreased with the decrease of the particle size (samples F1, F2, and F3 in Table 2). However, for samples F3, F4, and F5 that have similar particle

size but different volume packing fractions (i.e., different interparticle interactions), we have observed similar $\langle T_B \rangle$ values (Table 2). The decay of the reduced remanence, unlike to what is observed in the T_M values obtained from ZFC measurements, is mainly determined by the anisotropy, and thus, mean blocking temperatures are only slightly modified by interactions.[21,22] The standard deviation σ_y increased with both the particle size and the volume packing fraction (Table 2). This result agrees with the previously obtained result from the ZFC−FC curves, in which we observed an increase in the $T_S - T_M$ difference with both the particle size and the volume packing fraction.

Values of the effective magnetic anisotropy of the particles, K_{eff}, can provide information about the existence in addition to the magnetocrystalline anisotropy of other anisotropy terms, say, for example, surface and interface anisotropy. The value of K_{eff} was obtained from the magnetization data at 5 K using the law of approach to saturation:[28]

$$M = M_S\left(1 - \frac{B}{H^2} - \frac{C}{H^3}\right) + \chi_f H \qquad (3)$$

where M_S is the saturation magnetization, χ_f is the high-field susceptibility, and B is a function of M_S and K_{eff}, and for uniaxial polycrystalline structures is given by the following expression.[29]

$$B = \frac{4S_B K_{eff}^{\ 2}}{15M_S^{\ 2}} \qquad (4)$$

The fact that the obtained values (Table 2) are about 2 orders of magnitude larger than the bulk magnetocrystalline anisotropy constant ($K \approx 4.7 \times 10^4$ erg/cm^3) seems to suggest that the enhancement can be considered basically as coming either by surface or interface anisotropy contributions. Enhancements of 2 orders of magnitude in the anisotropy constant, associated with surface anisotropy, have already been observed in γ-Fe_2O_3 nanoparticles[8] and also in zinc ferrite nanoparticles.[3] The existence of a surface spin glasslike phase (i.e., magnetically disordered surface layer) has been suggested to be the reason for the high values of surface anisotropy in γ-Fe_2O_3 nanoparticles.[8] Supporting this result, the values of K_{eff} increase with the decrease of the particle size (samples F1, F2, and F3 in Table 2) and were similar for the samples with different volume packing fractions but similar particle size (samples F3, F4, and F5 in Table 2). In our system, shape anisotropy can be discarded because the nanocrystals are essentially spherical (Figure 2b). The thermal variation of the saturation magnetization of the composites followed a magnontype Bloch law for ferro- or ferrimagnets,[30] $M_S(T) = M_S(0)[1 - BT^b]$, where $M_S(0)$ is the saturation magnetization at $T = 0$ K and B and b are the Bloch constant and the Bloch exponent, respectively (Figure 5). Theoretical calculations on ferromagnetic clusters of Hendriksen et al.[31] show that a finite particle size can cause an increase in the Bloch exponent. Reduced coordination at the surface will cause the spins at the surface to be more susceptible to thermal excitation, which lead to larger dependences of the magnetization with temperature. However, values of b below, equal, and above 1.5 have been experimentally determined in nanocrystals.[3,32,33] In our samples, irrespectively of the packing fraction and particle size of the iron oxide nanocrystals, the Bloch exponent was similar to that of the bulk phase: $b = 1.5$, which suggests that the interaction between the nanoparticles and the silica matrix is weak.[33] Therefore, it seems that the main contribution to the anisotropy comes from the surface itself of the γ-Fe_2O_3 nanocrystals. This trend has been well-described

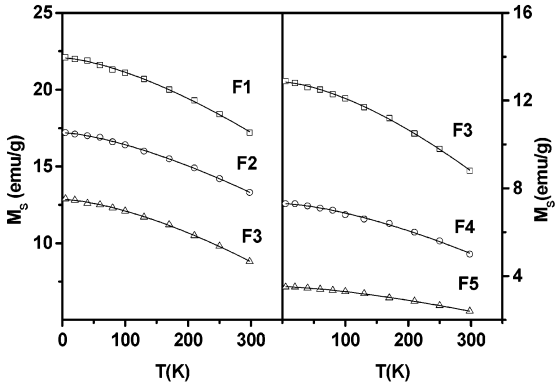

Figure 5. Variation of the saturation magnetization with temperature for all of the samples. The solid lines represent the best fit of the data to a magnontype Bloch law, $M_S(T) = M_S(0)[1 - BT^b]$.

for nanostructured ferrites of very different natures.[3,34−36] For coherent magnetization reversal of randomly oriented γ-Fe_2O_3 particles, values of the coercivity field of about 75 Oe are expected.[37] The values of H_C registered at 5 K (Table 2) are in all cases higher than this value, which indicates that the reversal process is not controlled by only magnetocrystalline anisotropy but rather by surface anisotropy. The presence of a disordered surface layer (responsible as above-mentioned of the enhancement of the anisotropy constant) that freezes below about 30 K has been associated with the significant enhancement of coercivity field values.[38]

Conclusions

Our studies revealed that the use of γ-Fe_2O_3 nanocrystals dispersed in submicrometer silica particles that were prepared by aerosol-assisted methods is especially appropriate to obtain information about the different factors that control the magnetic response of composites. In particular, we have determined that the magnetic response of these composites not only depends on the volume of the magnetic unit but also depends on the degree of dispersion of the magnetic nanocrystals within the diamagnetic matrix. We have also determined that interparticle interactions cause frustration of the moments and that the decay of the reduced remanence, unlike to what is observed in the ZFC experiments, is mainly controlled by the anisotropy. Finally, we have also concluded that the enhancement of the effective magnetic anisotropy with respect to the bulk γ-Fe_2O_3 can be considered as coming fundamentally from surface anisotropy.

Acknowledgment. Financial support from CICYT (PB98-0525) and PACTI (C001999-AX011) projects are gratefully acknowledged.

References and Notes

(1) Sun, S. H.; Murray, C. B.; Weller, D.; Folks, L.; Moser, A. *Science* **2000**, *287*, 1989.
(2) Rondinone, A. J.; Samia, A. C. S.; Zhang, Z. J. *J. Phys. Chem. B* **1999**, *103*, 6876.
(3) Hochepied, J. F.; Bonville, P.; Pileni, M. P. *J. Phys. Chem. B* **2000**, *104*, 905.
(4) Liu, C.; Zou, B.; Rondinone, A. J.; Zhang, Z. J. *J. Phys. Chem. B* **2000**, *104*, 1141.
(5) Rondinone, A. J.; Liu, C.; Zhang, Z. J. *J. Phys. Chem. B* **2001**, *105*, 7967.
(6) Liu, C.; Zhang, Z. J. *Chem. Mater.* **2001**, *13*, 2092.
(7) Morales, M. P.; Veintemillas-Verdaguer, S.; Montero, M. I.; Serna, C. J.; Roig, A.; Casas, Ll.; Martinez, B.; Sandiumenge, F. *Chem. Mater.* **1999**, *11*, 3058.
(8) Martinez, B.; Roig, A.; Molins, E.; González-Carreño, T.; Serna, C. J. *J. Appl. Phys.* **1998**, *83*, 3256.

(9) Liou, S. H.; Chien, C. L. *Appl. Phys. Lett.* **1988**, *52*, 512.
(10) Kumar, D.; Narayan, J.; Kvit, A. V.; Sharma, A. K.; Sankar, J. *J. Magn. Magn. Mater.* **2001**, *232*, 161.
(11) Katiyar, P.; Kumar, D.; Nath, T. K.; Kvit, A. V.; Narayan, J.; Shattopadhyay, S.; Gilmore, W. M.; Coleman, S.; Lee, C. B.; Sankar, J.; Singh, R. K. *Appl. Phys. Lett.* **2001**, *79*, 1327.
(12) Tartaj, P.; González-Carreño, T.; Serna, C. J. *Adv. Mater.* **2001**, *13*, 1620.
(13) Dormann, J. L.; Fiorani, D.; Tronc, E. *Adv. Chem. Phys.* **1997**, *98*, 283.
(14) Kemshead, J. T.; Treleaven, J. G.; Gibson, F. M.; Ugllstad, J.; Rembaum, A.; Philip, T. *Prog. Exp. Tumor Res.* **1985**, *29*, 249.
(15) Jung, C. W.; Jacobs, P. *Magn. Reson. Imaging* **1995**, *13*, 661.
(16) Gupta, P. K.; Hung, C. T. *Life Sci.* **1989**, *44*, 175.
(17) Ulman, A.; *Chem. Rev.* **1996**, *96*, 1533.
(18) Ennas, G.; Musinu, A.; Piccaluga, G.; Zadda, D.; Gatteschi, D.; Sangregorio, C.; Stanger, J. L.; Concas, G.; Spano, G. *Chem. Mater.* **1998**, *10*, 495.
(19) Tartaj, P.; González-Carreño, T.; Serna, C. J. *Langmuir* **2002**, *18*, 4556.
(20) Chantrell, R. W.; Popplewell, J.; Charles, S. W. *Physica 86*−*88B* **1977**, 1421.
(21) El-Hilo, M.; O'Grady, K.; Chantrell, R. W. *J. Magn. Magn. Mater.* **1992**, *114*, 295.
(22) Mørup, S.; Bødker, F.; Hendriksen, P. V.; Linderoth, S. *Phys. Rev. B* **1995**, *52*, 287.
(23) Cannas, C.; Casula, M. F.; Concas, G.; Corria, A.; Gatteschi, D.; Falqui, A.; Musinu, A.; Sangregorio, C.; Spano, G. *J. Mater. Chem.* **2001**, *11*, 3180.
(24) Cannas, C.; Concas, G.; Gatteschi, D.; Musinu, A.; Piccaluga, G.; Sangregorio, C. *J. Mater. Chem.* **2002**, *12*, 3141.
(25) Stoner, E. C.; Wohlfarth, E. P. *Philos. Trans. R. Soc. London, Ser. A* **1948**, *240*, 599.
(26) Bean, C. P.; Livingston, J. D. *J. Appl. Phys.* **1959**, *30*, 1205.
(27) Held, G. A.; Grinstein, G.; Doyle, H.; Sun, S.; Murray, C. B. *Phys. Rev. B* **2001**, *64*, 012408.
(28) Cullity, B. D. In *Introduction to Magnetic Material*; Addison-Wesley: Reading, MA, 1972; p 347.
(29) Kojima, H. In *Ferromagnetic Materials*; Wohlfarth, E. P., Ed.; North-Holland: Amsterdam, 1982; Vol. 3.
(30) Bloch, F. *Z. Phys.* **1931**, *61*, 206.
(31) Hendriksen, P. V.; Linderoth, S.; Lindgard, P. A. *J. Magn. Magn. Mater.* **1992**, *104*−*107*, 1577.
(32) Ngo, A. T.; Bonville, P.; Pileni, M. P. *J. Appl. Phys.* **2001**, *89*, 3370.
(33) Zhang, D.; Klabunde, K. J.; Sorensen, C. M.; Hadjipanayis, G. C. *Phys. Rev. B* **1998**, *58*, 14167.
(34) Moumen, N.; Pileni, M. P. *J. Phys. Chem.* **1996**, *100*, 1867.
(35) Moumen, N.; Pileni, M. P. *Chem. Mater.* **1996**, *8*, 1128.
(36) Prené, P.; Tronc, E.; Jolivet, J. P.; Livage, J.; Cherkaoui, R.; Nogues, M.; Dorman, J. L. *IEEE Trans. Magn.* **1993**, *29*, 2658.
(37) Bates, G. In *Ferromagnetic Materials*; Wohlfarth, E. P., Ed.; North-Holland: Amsterdam, 1980; Vol. 2, p 442.
(38) Martínez, B.; Obradors, X.; Balcells, L. I.; Rovanet, A.; Monty, C. *Phys. Rev. Lett.* **1998**, *80*, 181.